Available online at www.sciencedirect.com
SCIENCE DIRECT®
Journal of Catalysis 237 (2006) 337–348
JOURNAL OF CATALYSIS
www.elsevier.com/locate/jcat

Improving bifunctional zeolite catalysts for alkane hydroisomerization via gas phase sulfation

Christian Woltz, Andreas Jentys, Johannes A. Lercher *

Technische Universität München, Department of Chemistry, Lichtenbergstr. 4, D-85747 Garching, Germany

Received 15 July 2005; revised 5 November 2005; accepted 15 November 2005

Abstract

Pt-containing H-BEA zeolites were functionalized with sulfate anions via H_2S chemisorption followed by oxidation. This treatment generates sulfate groups and Brønsted acidic sites, modifies the supported metal particles, and leads to higher activity and selectivity for pentane hydroisomerization. The strength and the accessibility of the acid sites present in the parent material were not affected by this procedure. The concentration of Brønsted acidic sites and the catalytic activity for light alkane isomerization varied sympathetically. The parallel increase in isomerization selectivity indicates that either the residence time of the alkoxy intermediates decreases for the modified samples (suppressing undesired cracking reactions on the acid sites) or the selective decoration of the Pt particles with sulfur reduces hydrogenolysis on the metal particles.

Keywords: Isomerization; Pt/H-BEA; Sulfur treatment; Selectivity and activity; Acid sites

1. Introduction

Iso-pentane and branched hexanes are important components of high-octane motor fuels, which are produced via hydroisomerization of the *n*-alkanes over acidic catalysts. Mechanistically, hydroisomerization occurs in three elementary steps. First, the alkane is dehydrogenated. Then generated alkene adsorbs on a Brønsted acid site, forming an alkoxy group (a carbenium ion in the transition state), which isomerizes and eventually desorbs. Finally, the iso-olefin is hydrogenated to the iso-alkane. Therefore, catalysts are bifunctional, with a metal (Pt, Pd) catalyzing the hydrogenation/dehydrogenation step and an acidic function for the formation and isomerization of the alkoxy group/carbenium ion. The metal component also helps reduce catalyst deactivation by hydrogenating coke precursors.

As the reaction proceeds via carbenium ions, other Brønsted acid catalyzed reactions, such as oligomerization and cracking, compete with isomerization [1,2]. In addition, side reactions on the metal, such as hydrogenolysis of the alkane to smaller alkanes, may reduce the selectivity of the overall hydroisomerization reaction [3]. Eventually, the isomer yield is limited by the thermodynamic equilibrium between the iso- and *n*-isomers. Because branched alkanes are thermodynamically the more favored at lower reaction temperatures, the reaction temperature should be as low as possible. Consequently, catalysts active at low temperatures, such as heteropolyacids, sulfated or tungstated zirconia, and Pt on chlorinated Al_2O_3, have been explored [4–6]. Pt-containing catalysts based on zeolites operate at somewhat higher temperatures and thus limit the maximum yield achievable, but have the advantage of being less sensitive toward water and oxygenates. Currently, most industrial catalysts for isomerization of pentane and hexane are based on Pt/H-MOR as the catalytically active component, but new materials based on sulfated oxides have been commercially introduced [7,8].

Whether hydrogenation/dehydrogenation or the acid-catalyzed conversion is rate-determining depends on the concentration of the catalytic functions in the catalyst. At low concentrations of accessible metal atoms, their abundance determines the concentration of olefins and hence the catalytic activity. With a sufficient concentration of available metal surface atoms, hydrogenation/dehydrogenation becomes equilibrated. Under

* Corresponding author. Fax: +49 89 289 13544.
E-mail addresses: andreas.jentys@ch.tum.de (A. Jentys), johannes.lercher@ch.tum.de (J.A. Lercher).

0021-9517/$ – see front matter
doi:10.1016/j.jcat.2005.11.014

such conditions, the rate-determining step is the isomerization of the alkoxy groups/carbenium ions. Thus the concentration and strength of Brønsted acid sites determines the activity of the catalyst by controlling the concentration and lifetime of the alkoxy groups and the relative ratio of carbon–carbon bond cleavage versus isomerization [9]. The main focus for catalyst development lies on the modification of the acidic and textural properties of the catalysts. Examples of tailoring for that approach include the dealumination of zeolites and the partial ion exchange with divalent cations such as Zn^{2+} [10,11].

In this context, anion modification seems promising. Reports suggest that modification with $(NH_4)_2SO_4$ has a positive effect on the acidity and catalytic activity of zeolites [12]. The modification appears to involve formation of aluminum sulfate species. In this context, it is interesting to note also that sulfur oxide species appear to promote the activity for metal-catalyzed reactions [13–16].

With that in mind, we have modified Pt-containing zeolite by treatment with H_2S and subsequent oxidation and characterized the acid–base and catalytic properties of the novel zeolite-based bifunctional catalysts. This procedure ensures the generation of sulfur species close to the metal particles throughout the zeolite material and the subtle control of the overall and local concentration of the sulfate species formed in the new material.

2. Experimental

2.1. Catalyst preparation

Zeolite beta with a Si/Al ratio of 12.5 (H-BEA 25) was received from Süd-Chemie AG and was loaded with 1 wt% Pt by ion exchange with aqueous $Pt(NH_3)_4(OH)_2$ solution. A solution containing the appropriate amount of $Pt(NH_3)_4(OH)_2$ and an amount of NH_4OH corresponding to the theoretical amount of protons (competitive adsorption) in the sample was added dropwise to the slurry at 40 °C. After the ion exchange, the solid was centrifuged, washed, and freeze-dried. The samples were calcined in air 350 °C for 16 h (at a heating rate of 0.5 °C/min) and finally reduced at 300 °C in H_2 for 4 h. The metal loading after the preparation was determined using atomic absorption spectroscopy (AAS).

Pt-loaded ASA catalyst with a Si/Al ratio of 9.5 was synthesized using a mixture of acetic acid with $AlCl_3{\cdot}6H_2O$ (pH = 1.5) and sodium silicate solution (water glass; Merck) with NH_4OH (pH = 12). The solution was washed several times with ammonium acetate to eliminate Na^+ cations from the acidic support and finally calcined at 675 °C. Pt was impregnated using $Pt(NH_3)_4(OH)_2$ and subsequently calcined at 300 °C for 5 h and reduced with H_2 at 350 °C for 2 h.

For the sulfation procedure, the samples were heated in He atmosphere from room temperature to the sulfation temperature at a heating rate of 7.5 °C/min. Once the target temperature was reached, the sulfation procedure was initiated by passing a mixture containing 1.8 vol% H_2S in H_2 over the Pt-loaded zeolite at 350, 450, or 550 °C for 3 h at a WHSV of 2 $g_{H_2S}/(g_{cat}\,h)$. Subsequently, the material was oxidized in air for 3 h at a WHSV of 2 $g_{O_2}/(g_{cat}\,h)$. The three catalysts are identified as Pt/BEA S350, Pt/BEA S450, and Pt/BEA S550, respectively. Before characterization and kinetic testing, the samples were reduced in hydrogen for 90 min at 350 °C (heating rate, 5 °C/min).

2.2. Catalyst characterization

2.2.1. Hydrogen chemisorption

Hydrogen chemisorption was performed using a Sorptomatic 1990 series instrument. About 1 g of catalyst was reduced in hydrogen at 350 °C for 2 h and subsequently evacuated. All adsorption isotherms were measured at 35 °C. The amount of chemisorbed hydrogen was determined after physisorbed hydrogen was removed from the sample by evacuation at 35 °C and determining that fraction quantitatively by repeating the exposure and measuring the uptake. The isotherm of chemisorbed hydrogen was determined by subtracting the second isotherm (containing only physisorbed H_2) from that measured in the first experiment (containing chemisorbed and physisorbed H_2). The monolayer coverage of hydrogen adsorbed was determined by extrapolating the linear part of the adsorption isotherm to zero pressure. The fraction of metal surface atoms was calculated by assuming the adsorption of one hydrogen atom per Pt surface atom.

2.2.2. X-Ray absorption spectroscopy

The structural and chemical properties were investigated by X-ray absorption spectroscopy (XAS) measured on beamline X1 at Hasylab, DESY, Hamburg. The storage ring DORIS III operates with a positron energy of 4.5 GeV and a current between 85 and 51 mA. X-Ray absorption spectra were recorded at the Pt L_{III} edge (11564 eV) in transmission mode, using a stepwise moving Si (111) monochromator. The intensity of incident and transmitted X-rays were recorded using ionization chambers. The monochromator was detuned to 60% of the maximum intensity, to avoid contributions of high harmonics in the X-ray beam. The samples were pressed into self-supporting wafers and placed in the sample holder equipped with a heating and cooling system. Activation and reduction of the samples was carried out in hydrogen for 2 h at 350 °C. The spectra were measured at liquid nitrogen temperature.

For EXAFS analysis, the oscillations were extracted from the background using a second-order polynomial function, and after weighting with k^2, the oscillations were Fourier-transformed in the range of 3–13 $Å^{-1}$. The local environment of the Pt atoms was determined from the analysis of the EXAFS in k-space applying phase-shift and amplitude functions for Pt–Pt and Pt–S calculated assuming multiple scattering processes (FEFF version 8.10 [17]) using the Viper program [18].

2.2.3. Ion chromatography

The amount of sulfate species present on the samples was determined by liquid ion chromatography (Metrohm 690) using an anion column IC SUPER-SEP with phthalic acid (2.5 mmol/l) and 5% acetonitrile as eluents. For determining the sulfate content, 20 mg of catalyst was dissolved in 100 ml of sodium hydroxide (0.01 mol/l).

2.2.4. N_2 adsorption

The specific surface areas and pore volumes were determined by physisorption of nitrogen using a Sorptomatic 1990 series instrument. About 500 mg of the sample was heated to 350 °C and evacuated for 1 h before nitrogen adsorption was carried out at a temperature of −196 °C. The specific surface area was calculated according to the Brunauer–Emmett–Teller (BET) method. The pore volume was determined using the t-plot method.

2.2.5. Temperature-programmed desorption

Temperature-programmed desorption (TPD) was performed in a home-built 6-fold parallel TPD system. The catalysts were activated by heating in vacuum to 350 °C (at a rate of 10 °C/min) for 2 h. Ammonia was adsorbed at 150 °C with a partial pressure of 0.6 mbar for 1 h, and then the samples were evacuated at 10^{-3} mbar for 2 h to remove physisorbed molecules. For the TPD experiments, the 6 samples were (sequentially) heated from 150 to 800 °C at a rate of 10 °C/min, and the species desorbing were monitored by mass spectrometry (MS), using a Balzers QME 200. In each set of experiments, a reference sample with known concentration of acid sites was used to calibrate the MS signal.

2.2.6. Infrared spectroscopy

Infrared (IR) spectra after adsorption of pyridine were measured from 3800 to 1100 cm^{-1} at a resolution of 4 cm^{-1} using a Perkin–Elmer 2000 spectrometer and a heatable high-vacuum IR cell as described previously [19]. A self-supporting wafer was activated by heating in vacuum at a rate of 10 °C/min to 350 °C and maintaining that temperature for 60 min. After the sample was cooled to 150 °C, the spectrum of the activated zeolite was recorded. Pyridine was adsorbed at 150 °C with a partial pressure of 0.05 mbar for 30 min, and the sample was subsequently evacuated at that temperature until IR spectra recorded at 10-min intervals did not vary. To compare the spectra of the different samples, all spectra were normalized by the intensity of the lattice vibration overtones of the zeolite between 1750 and 2100 cm^{-1}. To determine the concentration of Brønsted and Lewis acid sites according to the method published by Emeis [20], the weight of the wafers was used.

In situ IR measurements during sulfur treatment and C_5 isomerization were carried out using a flow cell equipped with ZnS windows and a resistance-heated furnace for the sample holder. For in situ IR experiments, the samples were pressed into self-supported wafers (ca. 2 mg) and activated for 90 min at 350 °C in hydrogen. For H_2S and oxidation treatment, a flow of 20 ml/min was used.

2.2.7. Temperature-programmed reduction studies

Temperature-programmed reduction (TPR) studies were performed in a flow reactor system heated with a cylindrical ceramic oven equipped with 3 × 1000 W of thermal output (Horst GmbH). The gases evolved during TPR were monitored by MS (Balzers QME 200). For activation, the samples were heated in He atmosphere from room temperature to 375 °C at a rate of 5 °C/min, and this temperature was maintained for 90 min.

2.3. Catalytic reactions

The catalytic activity was studied with a 20-fold parallel plug flow reactor system. The reactant gas flow and pressure of each reactor were controlled by individual digital mass flow controllers and back-pressure regulators. The liquid feed was adjusted and mixed with hydrogen using a digitally controlled evaporator–mixer. For analysis of the products, an HP MicroGC (GC M200), capable of separating aliphatic C_1–C_6 hydrocarbons (including their isomers) in <2 min, was used. The total pressures, flow rates, temperatures, and alkane concentrations were varied automatically. For the kinetic experiments, external diffusion limitations were experimentally excluded, and the activity was determined under differential reaction conditions. All data recorded were stored in a relational MS access database.

The rate constant for the formation of iso-C_5 (k_{iso}) was calculated from the concentration of n-C_5 in the feed (n-C_5^{feed}), and after the reactor (n-C_5^{exit}), the selectivity to iso-C_5 ($S_{iso.C_5}$) and the catalyst mass (m_{cat}) according to

$$k_{iso} = \frac{\text{Flow} \cdot \ln(n\text{-}C_5^{feed}/n\text{-}C_5^{exit}) \cdot S_{iso.C_5}}{m_{cat}}.$$

The reaction order for pentane was experimentally determined to be $n_{C_5} = 1$.

3. Results

3.1. Preparation procedure and sulfate loading

In principle, sulfate ions could be introduced into a zeolite via several approaches, including direct impregnation with ammonium sulfate, sorption of SO_3 (including the oxidative sorption of SO_2), and sorption of H_2S or an organic sulfide with subsequent oxidation. We have opted for the latter route, because it provides the most subtle method of introducing sulfates and modifying zeolite acidity without inducing damage to the structure or generating high local concentrations of sulfates. The method that we applied used the equilibration with H_2S in hydrogen at several temperatures to ensure equilibration of the metal particles with sulfur at the accessible Pt surface and its subsequent oxidation to SO_3, which was trapped by the aluminum oxide nanoclusters in the zeolite pores.

With increasing temperature of the equilibration with H_2S, the overall retention of sulfur in the material decreased (see Table 1). Because the retention of sulfur originally occurs via the formation of Pt sulfide species, the results indicate that the most sulfur is retained at the lowest reaction temperature, in line with the decreasing stability of Pt sulfide with increasing temperature. Whereas the content of sulfate species was in the same order of magnitude than the concentration of acid sites for a sulfation temperature of 350 °C, it was significantly reduced at higher temperatures (see Table 1). Note that using the concentration of sulfur bound as PtS, the maximum amount of sulfur deposited in one step should not be >0.05 mmol per gram of zeolite for a single preparation step. It is interesting to note

Table 1
Concentration of acid sites, sulfate concentration, fraction of Pt surface atoms and specific surface area of Pt/BEA after sulfur treatment at different temperatures

Sample	Brønsted acid sites (mmol/g)	Lewis acid sites (mmol/g)	SO_4^{2-} content (mmol/g)	SO_4^{2-}/Pt (mol/mol)	Surface Pt atoms (H/Pt)	Pore volume (cm^3/g)
Pt/H-BEA	0.28	0.28	–		0.52	110
Pt/BEA S350	0.39	0.29	0.44	8.7	0.11	102
Pt/BEA S450	0.32	0.27	0.14	2.6	0.06	105
Pt/BEA S550	0.24	0.21	0.06	1.2	<0.01	95

that this is about the concentration retained at the highest reaction temperature (see Table 1). As the amount of sulfur retained decreased with increasing temperature, the results suggest that at 350 °C, either more than one sulfur atom was retained per accessible Pt atom or H_2S was adsorbed not only on Pt, but also on the zeolite acid sites similar to what has been observed for H_2S adsorption on H-ZSM5 [21]. At the highest equilibration and oxidation temperature, the concentration of the sulfate species was equal to the concentration of Pt, suggesting that the more weakly bound H_2S fraction retained on the support was not stable during the sulfation and oxidation treatment at this temperature.

3.2. Characterization of the metal particles

Because the various treatments and the use of the catalyst in a strongly reducing atmosphere could lead to marked modification of the metal particles, we took great care to characterize the concentration of accessible Pt atoms, as well as the size and electronic state of the particles. We used hydrogen chemisorption to assess the concentration of accessible Pt atoms. The results are summarized in Table 1. For the parent Pt/BEA with 1 wt% Pt, the H/Pt ratio was determined to be 0.5. The concentration of accessible Pt atoms that adsorbed hydrogen was severely reduced after the sulfur treatment, with a more pronounced decrease seen with increasing S-treatment temperature. For sample Pt/BEA S550, the concentration of accessible Pt dropped below the detection limit.

XAS was applied to explore the electronic and structural features of the Pt particles [22]. The XANES of Pt/BEA before and after sulfur treatment are compared with that of a Pt foil in Fig. 1. For the untreated catalyst, the intensity of the peak above the absorption edge (white line) was smaller compared with that of the Pt foil. The sulfur treatment at 350 °C led to an increased intensity of the white line compared with that of parent Pt/BEA. For samples Pt/BEA S450 and Pt/BEA S550, the intensity of the white line was further increased. The additional peak at 17 eV above the Pt L_{III} edge (assigned to multiple scattering contributions) increased in intensity with increasing temperature of the sulfur treatment. For the parent sample and sample Pt/BEA S350, only a small peak was observed, whereas for samples Pt/BEA S450 and Pt/BEA S550, a well-defined peak developed at 17 eV above the Pt L_{III} edge. This peak is considered part of the EXAFS oscillations, and hence its increase suggests an increase in particle size.

The radial distribution functions of Pt for Pt/BEA catalysts before and after sulfur treatment are compared in Fig. 2, and the results of the analysis of the EXAFS are summarized in Table 2. The parent material shows Pt–Pt contributions of the first coordination shell (approximately 2.7 Å) and a minor contribution of the second coordination shell (approximately 3.9 Å). The sample Pt/BEA S350 showed the same contributions for Pt–Pt scattering and additional Pt–S contributions around 2 Å,

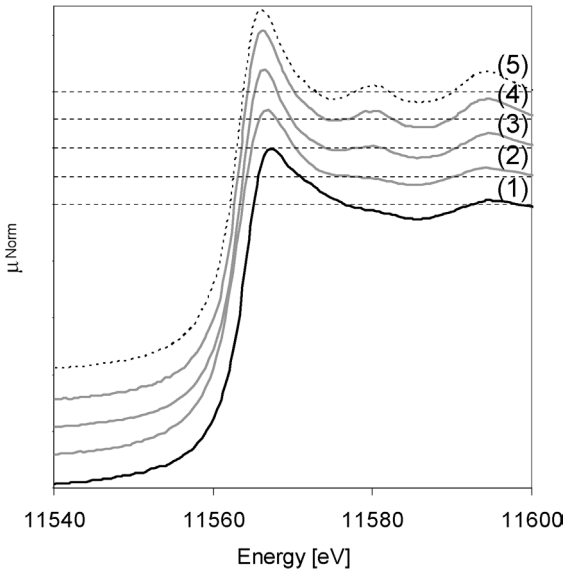

Fig. 1. (a) XANES for Pt/BEA (—) (1), H_2S and air treated (—) Pt/BEA S350 (2), Pt/BEA S450 (3), Pt/BEA S550 (4) and Pt-foil (···) (5).

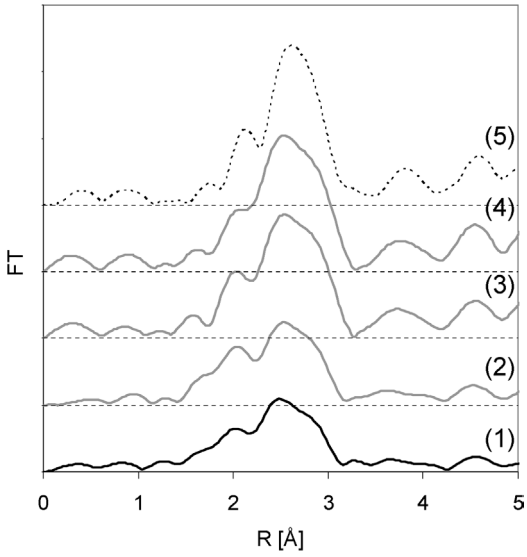

Fig. 2. Fourier transformed EXAFS (k^2-weighted) for Pt/BEA (—) (1), H_2S and air treated (—) Pt/BEA S350 (2), Pt/BEA S450 (3), Pt/BEA S550 (4) and Pt-foil (···) (5).

Table 2
Results of the analysis of the EXAFS for Pt/BEA before and after the sulfur treatment

Sample	Shell	Number of neighbors[a]	Distance[b] (Å)	DW factor[c] (Å)	E_0 correction[d] (eV)
Pt/BEA	Pt–Pt	8.3	2.74	6.4×10^{-3}	8.4
Pt/BEA S350	Pt–Pt	8.3	2.75	6.1×10^{-3}	8.3
	Pt–S	0.98	2.29	5.2×10^{-2}	8.8
Pt/BEA S450	Pt–Pt	10.1	2.76	4.2×10^{-3}	9.4
	Pt–S	0.91	2.25	1.6×10^{-3}	3.9
Pt/BEA S550	Pt–Pt	11.3	2.76	5.0×10^{-3}	8.9

[a] Coordination number of the absorber–backscatter pair.
[b] Average absorber–backscatter distance.
[c] Debye–Waller factor.
[d] Inner potential correlation.

indicating formation of a direct bond between Pt and sulfur. The Pt–Pt contributions in the first (∼2.7 Å) and second coordination shells (∼3.9 Å) increased for samples Pt/BEA S450 and Pt/BEA S550, indicating growth of the Pt particles, whereas the Pt–S contribution was more pronounced at lower temperatures during sulfur treatment.

3.3. Characterization of the zeolite and sulfate component

XRD of the zeolite samples showed no variations in zeolite crystallinity after the sulfur treatment; that is, the materials were identified as polymorph BEA without changes in the intensity or location of the diffraction peaks induced by the treatments. Additional peaks were not observed, indicating that, if formed, other phases were either X-ray amorphous or below the detection limit.

TPD of NH_3 from Pt/BEA after sulfur treatment at different temperatures and that of the parent catalyst is shown in Fig. 3. Two overlapping peaks for NH_3 desorption were seen, indicating the presence of two sorption states of ammonia. For the parent material, the peaks occurred at 350 and 550 °C. The maximum at lower temperature did not vary significantly with treatment, whereas that at higher temperature shifted to 480 °C, indicating decreasing strength of acid site interactions after sulfation. The amount of ammonia desorbed in sample Pt/BEA S350 was markedly higher than that in the parent sample. The amount of ammonia desorbed in sample Pt/BEA S450t was higher than that in the parent sample but lower than that in sample Pt/BEA S350, and that in sample Pt/BEA S550 was lower than that in the parent sample.

The IR spectra of Pt/BEA and of the sulfur-treated samples before and after pyridine adsorption are shown in Fig. 4. For sample Pt/BEA S350, the intensity of the band at 3608 cm^{-1} (strong Brønsted acid sites) increased by 15% compared with the parent material. For sample Pt/BEA S450, the intensity was approximately identical, and for sample Pt/BEA S450, the intensity of the band at 3608 cm^{-1} was less than that of the parent material. The formation of additional silanol groups at 3733 cm^{-1}, assigned to SiOH groups at defects, was observed with the samples treated at 450 and 550 °C. Pyridine adsorption led to the disappearance of the bands at 3608 and 3785 cm^{-1}, assigned to Brønsted acidic hydroxyl and AlOH groups, respectively, and to a decreased intensity of the silanol groups at 3743 cm^{-1}, indicating that all hydroxyl groups were accessible for pyridine and that the sulfur treatment did not cause pore blocking.

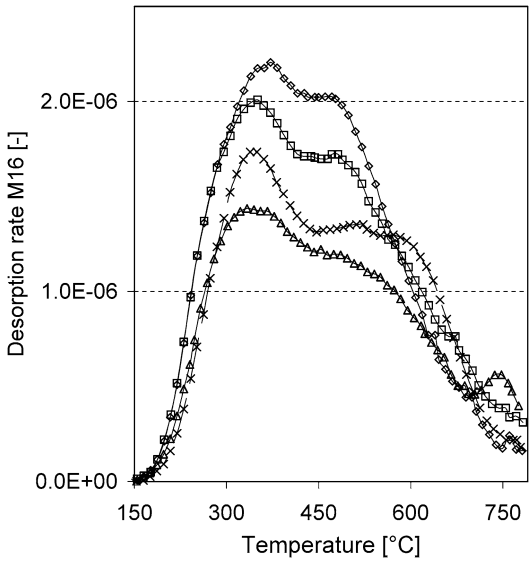

Fig. 3. NH_3-TPD of Pt/BEA (×), Pt/BEA S350 (◇), Pt/BEA S450 (□) and Pt/BEA S550 (△).

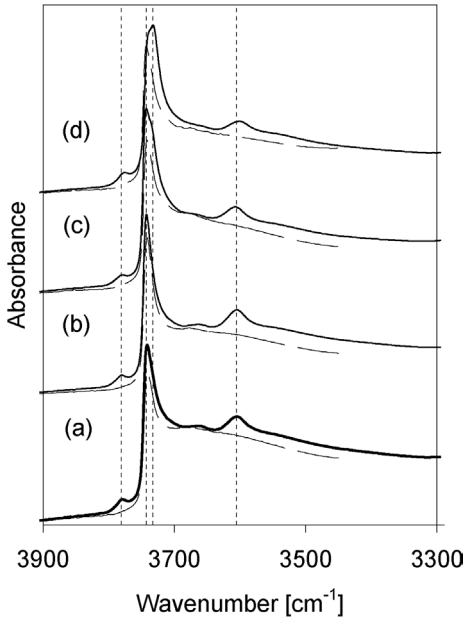

Fig. 4. IR spectra of activated Pt/BEA (a) (—), H_2S and air treated (—) Pt/BEA S350 (b), Pt/BEA S450 (c), Pt/BEA S550 (d) and after pyridine adsorption (—) (normalized to the lattice vibrations between 1750 and 2100 cm^{-1}).

The IR spectra before and after pyridine adsorption of the parent Pt/BEA material and the samples after sulfur treatment at different temperatures are shown in Fig. 5. The typical bands of pyridine ring vibrations (1544 cm^{-1} for pyridine on Brønsted sites, 1490 cm^{-1} for pyridine interacting with Brønsted and Lewis sites, and 1455 cm^{-1} for pyridine on Lewis sites) were observed for all materials. Quantitative evaluation of the pyridine ring vibrations revealed that the concentrations of pyri-

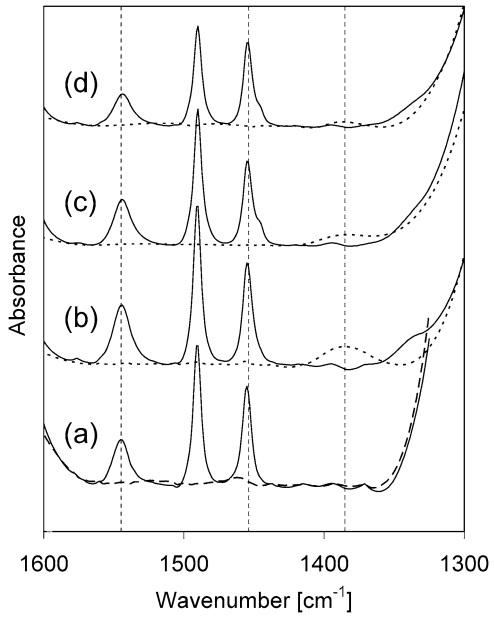

Fig. 5. IR spectra of (—) activated Pt/H-BEA (a), Pt/BEA S350 (b), Pt/BEA S450 (c), Pt/BEA S550 (d) and after pyridine adsorption (—) (normalized to the lattice vibrations between 1750 and 2100 cm^{-1}).

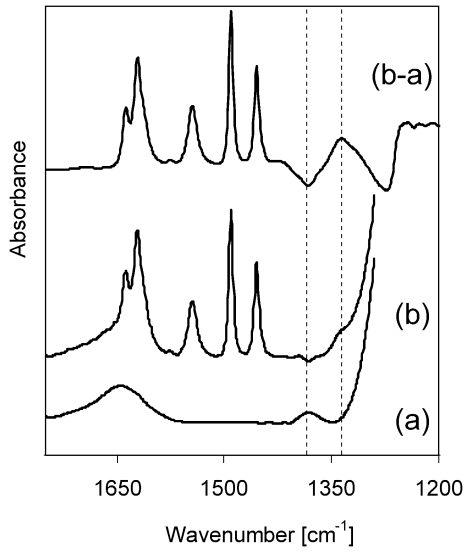

Fig. 6. IR spectra of activated Pt/BEA S350 (a), after adsorption of pyridine (b) and difference spectra (b − a) (normalized to the lattice vibrations between 1750 and 2100 cm^{-1}).

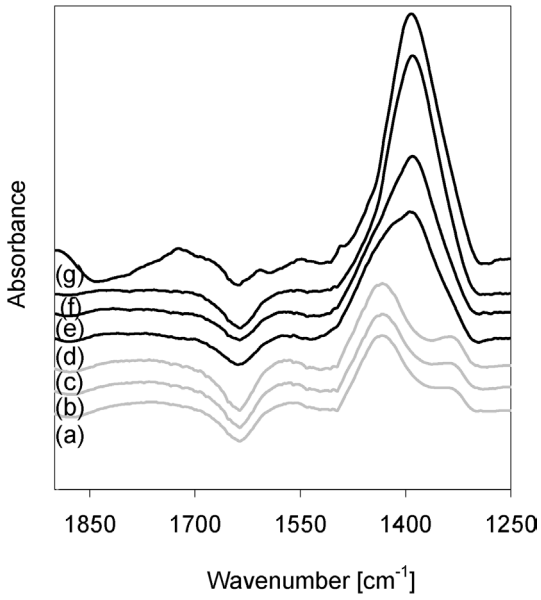

Fig. 7. Difference in situ IR spectra during H_2S treatment (—) after (a) 1, (b) 6 and (c) 90 min and oxidation (—) (d) 1, (e) 2, (f) 40 and (g) 60 min.

dinium ions and of Lewis acid-coordinated pyridine varied considerably (see Table 1). Sulfur treatment at low temperatures led to higher concentrations of Brønsted acid sites, while the concentration of Lewis acid sites remained constant. With increasing treatment temperature, the concentration of Brønsted and Lewis acid sites decreased. Pt/BEA S450 showed reduced Brønsted and Lewis acid site concentrations. The shoulder at the band at 1455 cm^{-1} at lower wavenumbers indicates the formation of a minor fraction of strong Lewis acid sites, which can be assigned to extra-framework Al species formed during the sulfation at higher temperatures. In addition, the concentration of sulfate on the samples decreased with increasing sulfur treatment temperature (as measured by ion chromatography). The band observed at 1385 cm^{-1}, assigned to surface sulfate species [23,24], decreased with increasing H_2S/oxidation treatment temperature and was not observed for the parent material. It should be noted that the concentration of sulfate on the sample is on the same order of magnitude as the concentration of acid sites for the sample sulfated at low temperatures, whereas at a sulfation temperature of 550 °C, the concentration of sulfate species is reduced by almost a factor of 10. Comparing these variations in the concentrations of sulfates and Brønsted and Lewis acid sites, it is evident that any sulfate groups deposited may influence, but not generate, the majority of the acid sites.

The differences in the IR spectra before and after adsorption of pyridine on Pt/BEA S350 are compared in more detail in Fig. 6. After adsorption of pyridine, the band at 1385 cm^{-1}, assigned to the stretching frequency of a covalent S=O bond, was reduced and a new band at 1335 cm^{-1}, assigned to the S=O stretching vibration perturbed by pyridine, was observed. This indicates that the basic molecule interacted (directly or indirectly) with the sulfate group, similar to what has been observed for the sulfate groups of sulfated zirconia [25].

3.4. Nature of sulfate species under reaction conditions

In situ IR measurements of the Pt/H-BEA catalyst at 350 °C during H_2S treatment and oxidation are shown in Fig. 7. During H_2S treatment in hydrogen atmosphere, bands at 1445 and 1330 cm^{-1} were observed, whereas during oxidation in air, an intense band at 1385 cm^{-1} was formed. Note that the catalyst was stored in air, and thus bands assigned to S=O vibrations were already present after the H_2S treatment. In accordance with earlier work [26,27], the band at 1330 cm^{-1} can be attributed to SO_2 physisorbed on alumina. The band at 1145 cm^{-1}, which should also appear with physisorbed SO_2,

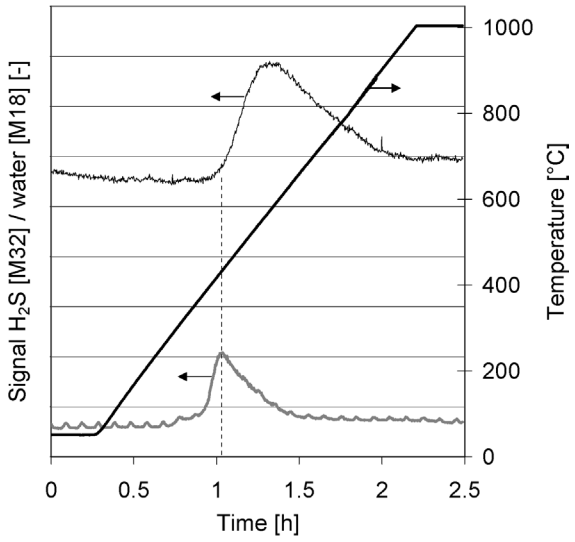

Fig. 8. Temperature programmed reduction of Pt/BEA S350 (temperature (—), evolution of H_2S (—) and water (—)).

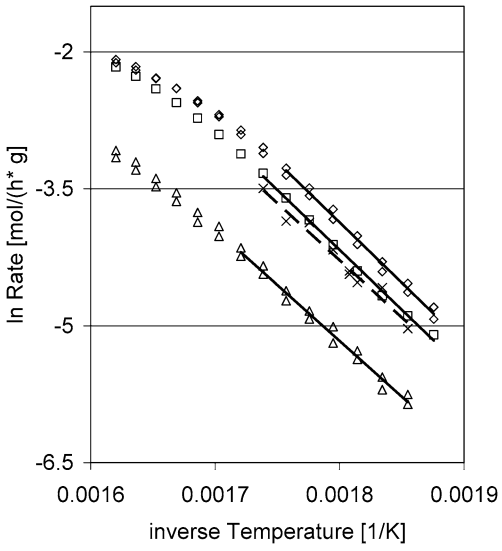

Fig. 9. Isomerization activity of Pt/BEA (104 kJ/mol) (×, - - -), Pt/BEA S350 (110 kJ/mol) (◇, —), Pt/BEA S450 (109 kJ/mol) (□, —) and Pt/BEA S550 (102 kJ/mol) (△, —).

was masked by strong bands of the zeolite lattice vibrations. Note that a band around 1400 cm^{-1} was assigned to strongly bound sulfate species on magnesium-alumina spinels [28] and on MgO [26] exposed to SO_2/O_2. The small band at 1445 cm^{-1} was tentatively attributed to molecular sulfuric acid [23]. SH stretching vibrations at 2560 cm^{-1} as observed in earlier work [21] after adsorption of H_2S on Na-ZSM5 were not detected.

To analyze the stability of the sulfate species on the surface of the catalysts, TPR measurements were carried out for Pt/BEA S350. The sample was activated in He at 350 °C for 90 min before the TPR to remove all physisorbed water. During the reduction in H_2, the sample was heated to 1000 °C at a rate of 7.5 K/min. The H_2S signal during TPR is shown in Fig. 8. H_2S began to desorb above 380 °C, reaching a maximum at 440 °C. At 440 °C, the formation of water was observed, which we attributed to decomposition of the sulfate species. In turn, this high temperature of decomposition indicates that the sulfate species were stable under the reaction conditions applied for the isomerization reaction.

3.5. Hydroisomerization of pentane

Fig. 9 shows the catalytic activity of the parent Pt/BEA and the samples sulfated at a total pressure of 4 bar, a WHSV of 30 h^{-1}, and temperatures of 260–350 °C in the form of an Arrhenius plot. In general, a higher isomerization rate was observed with decreasing sulfation temperature. The comparison of the activities of the parent and modified catalysts in the kinetic regime (linear part at low temperatures) shows the positive effect of the milder treatments (Pt/BEA S350, Pt/BEA S450). Increasing the sulfation temperature to 550 °C, on the other hand, leads to a reduction of the isomerization rate compared with that of the parent material. The apparent activation energies varied between 102 and 110 kJ/mol. The very subtle variations in the apparent energy of activation and the larger variation of the composed preexponential factor suggest that

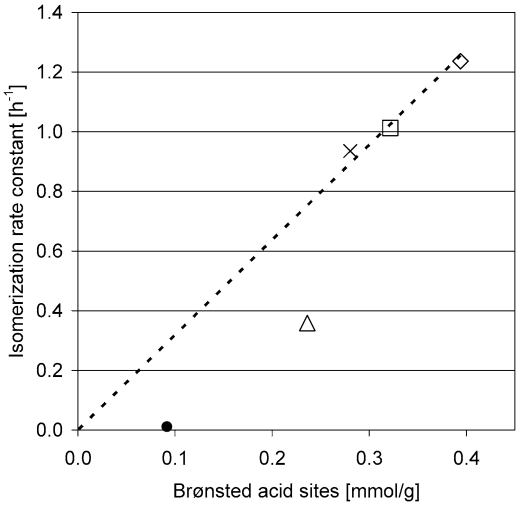

Fig. 10. Correlation of Brønsted acidity and isomerization activity for Pt/BEA (×); Pt/BEA S350 (◇), Pt/BEA S450 (□), Pt/BEA S550 (△) and for Pt-ASA (●).

the main effect of the sulfate treatment resulted in a variation in the concentration of the (Brønsted) acid sites. This is nicely illustrated by the linear correlation between the concentration of Brønsted acid sites and the isomerization activity, as shown in Fig. 10. The direct correlation indicates that, as expected, the reaction of intermediately formed olefins on the Brønsted acid sites controls the kinetics of the reaction; that is, normalized to Brønsted acid sites, the parent and Pt/BEA S350 and Pt/BEA S450 have the same catalytic activity. The lower than expected activity for Pt/BEA S550 can be attributed to the very low concentration of accessible Pt atoms in this sample. For this catalyst, the concentration of accessible Pt atoms is so low that it influences or controls the catalytic activity. Fig. 11 shows the iso-pentane selectivity at various conversion levels (with WHSV of 5–30 h^{-1}), a temperature of 300 °C, and a total pressure of 4 bar ($H_2/C_5 \approx 30$). It also shows the maximum selec-

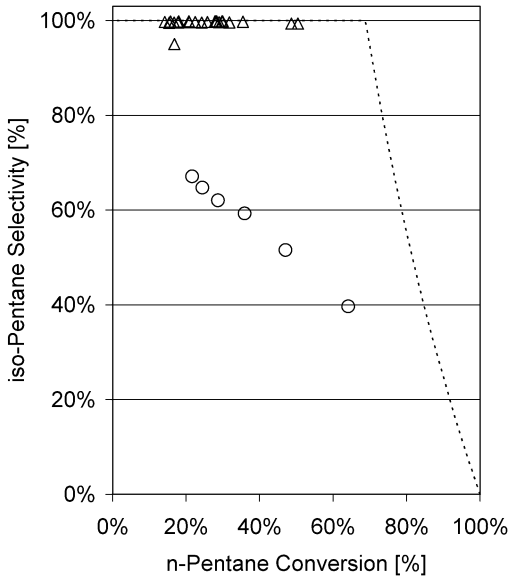

Fig. 11. Selectivity to iso-pentane at 300 °C for Pt/BEA (○) and Pt/BEA S350 (△); equilibrium at 300 °C (- - -).

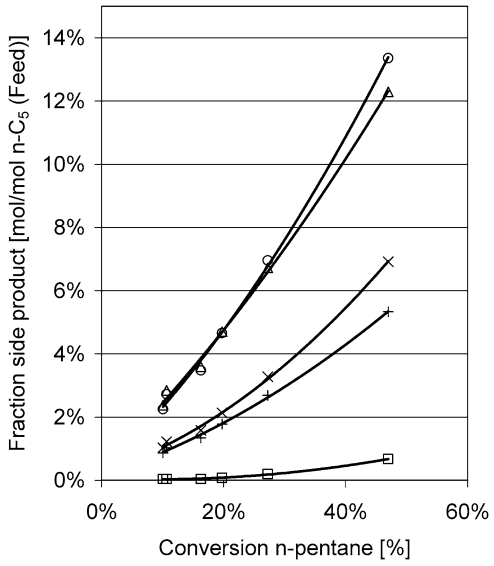

Fig. 12. Product distribution for Pt/BEA methane (×), ethane (○), propane (△), iso-butane (□) and *n*-butane (+) at 300 °C.

tivity achievable at a given conversion level due to the thermodynamic equilibrium between *n*- and iso-pentane at 300 °C. (At this temperature, the equilibrium-constant K between iso-C_5 and *n*-C_5 was experimentally determined to be 2.2.) The thermodynamic equilibrium between *n*- and iso-pentane at 300 °C (the upper limit for the achievable selectivity) is also included in this figure. The iso-pentane selectivity of the untreated catalyst decreased sympathetically with increasing conversion, whereas after sulfation, the selectivity reached almost 100% independent of the conversion level until thermodynamic equilibrium was reached.

The main side reaction under the conditions studied was C–C bond cleavage. Products from oligomerization (i.e., hydrocarbons $>C_5$) were observed in only negligible concentrations. The typical distribution of the products at 300 °C for Pt/BEA resulting from C–C bond-breaking reactions is given in Fig. 12. A symmetric distribution of C_2 and C_3 and of C_1 and C_4 alkanes independent of the conversion level was observed. The concentration of the primary products ethane/propane and methane/butane were nearly equal. At higher temperatures, the concentration of C_1 increased as a result of enhanced activity for secondary C–C bond-breaking reactions. Sulfation treatment did not influence the product distribution of the cracking/hydrogenolysis reactions. Only low concentrations of isobutane were found, resulting from a consecutive reaction (the zero initial slope at zero conversion).

Fig. 13 shows the logarithmic rate of the formation of the side products versus the inverse reaction temperature. In the low-temperature region, a linear relationship of the rate of formation of side products and the inverse temperature was observed. Whereas at low temperatures, the distribution of the products was the same as for the reaction conditions used in Fig. 12, at higher temperatures (and thus closer to the equilibrium concentrations), the formation of *n*- and iso-butane decreased due to consecutive reactions. The apparent activation energies measured below 300 °C (linear region) are given in Fig. 13. Ethane and propane had similar apparent activation energies (about 110 kJ/mol), indicating that both products were formed in parallel. The apparent energies of activation of methane and *n*-butane were higher, suggesting a different pathway of formation or a different sorption state of the precursor.

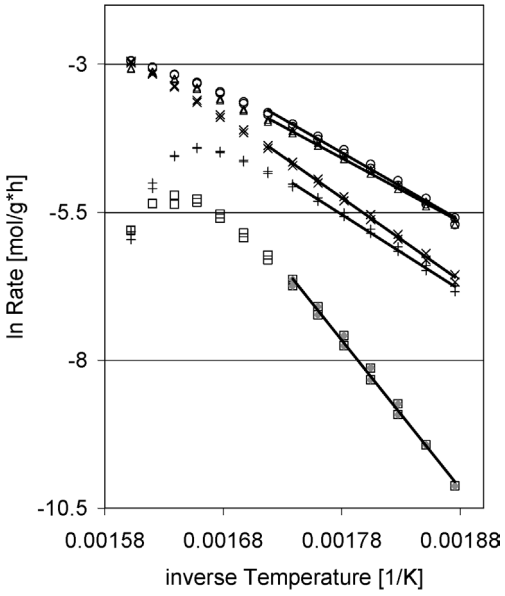

Fig. 13. Arrhenius plot for Pt/BEA: methane (E_A = 138 kJ/mol) (×), ethane (E_A = 113 kJ/mol) (○), propane (E_A = 106 kJ/mol) (△), iso-butane (E_A = 250 kJ/mol) (□) and *n*-butane (E_A = 125 kJ/mol) (+).

To explore the kinetics of the side reactions on a catalyst with very low concentration of acid sites, *n*-pentane conversion was carried out on a Pt-loaded silica alumina catalyst with 0.8 wt% platinum. The low concentration of acid sites (0.065 mmol H^+/g) induced only low activity for acid-catalyzed isomerization and cracking reactions. The product distribution (Fig. 14) showed only a low concentration of iso-

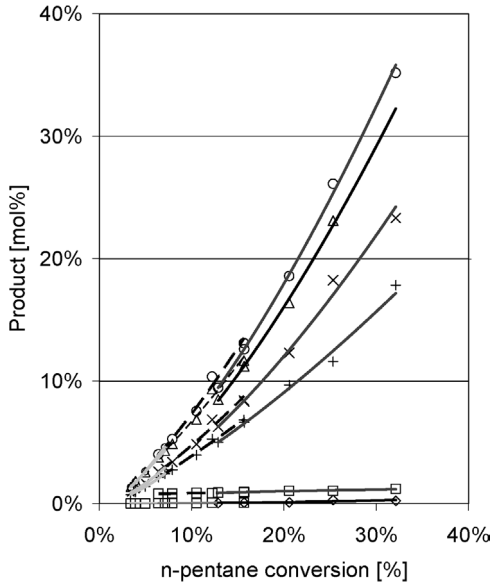

Fig. 14. Product distribution for Pt-ASA: methane (×), ethane (○), propane (△), iso-butane (◇), *n*-butane (+) and iso-pentane (□); at 280 °C (—), 300 °C (- - -) and 320 °C (—).

pentane, indicating that the acid-catalyzed isomerization hardly occurred at the space velocity used. This suggests that with this catalyst, lighter alkanes were formed primarily from metal-catalyzed reactions. The experiment was carried out at 280, 300, and 320 °C, to cover a wide conversion range with weight hourly space velocities of 5 and 30 h^{-1}. Fig. 14 shows that the temperature did not severely affect the product distribution, indicating that all products had approximately the same apparent energy of activation. Ethane and propane, as well as methane and *n*-butane, evolved in parallel and with identical molar concentrations. Iso-butane was observed to only a negligible extent. The product distribution for these lighter alkanes resembles that of Pt/BEA (see Fig. 12), with the exception of the same apparent energy of activation for all light alkanes. It is also noteworthy that the perfect linear dependence between product yields and overall conversion suggests that the transformation of products does not play a significant role.

4. Discussion

4.1. Influence of sulfur treatment on metal properties

Hydrogen chemisorption and XAS measurements at the Pt_{III} edge were used to explore the effects of sulfation on Pt. For the parent Pt/BEA, hydrogen chemisorption showed that the fraction of Pt atoms exposed was approximately 0.5. Assuming spherical Pt particles, this suggests an average particle size of about 25 Å. However (still assuming spherical particles), the average coordination number of Pt in the first shell ($N_{Pt–Pt} = 8.3$) suggests an average particle size of 15 Å and, consequently, exposure of approximately 70% of the Pt atoms [22,29]. In line with our earlier conclusions regarding a similar difference between the fraction of surface atoms measured by H_2 chemisorption and derived from EXAFS analysis, we attribute this difference to the restricted access of H_2 to the Pt particles within the zeolite pores [30].

Treatment with H_2S and subsequent oxidation results in a significantly decreased fraction of metal surface atoms able to chemisorb H_2 at all treatment temperatures. Both the EXAFS coordination number and the intensity of the peak at 17 eV above the Pt L_{III} edge suggest that the size of the metal particles remains unaffected after sulfation at 350 °C (Pt/BEA S350). But the higher coordination numbers for Pt–Pt determined from the EXAFS analysis and the more pronounced peak at 17 eV above the Pt L_{III} edge indicate sintering of the metal particles during treatment at 450 and 550 °C. Thus, we conclude that the treatment with H_2S and the subsequent oxidation lead to blocking of a significant fraction of the surface atoms by sulfur. In addition to this, the Pt particles sinter to an increasing extent as the treatment temperature is raised to 450 and 550 °C.

It should be noted that the increase of the peak above the absorption edge (white line) with increasing severity of the treatment could result from particle size effects or from changes in the electron density on the metal. Because the greatest white line intensity was observed for the Pt foil (largest particle size) and white line intensities varied in parallel to particle size, we tentatively attribute the intensity changes to particle size effects. Note that the similar particle size in the parent and Pt/BEA S350 allows us to conclude that a small increase in the white line after sulfur treatment is due to a slight degree of electron withdrawal from the Pt particles.

EXAFS of Pt/BEA S350 showed the presence of Pt–S contributions. Using a metal dispersion of 50% for the sample Pt/BEA S350 and the average number of Pt–S direct neighbors $N_{Pt–S} = 0.98$, we conclude that every Pt surface atom is in direct contact with two sulfur atoms. The short distance between Pt and S (∼2.27 Å) indicates the presence of Pt-sulfide species [31], suggesting that the sintering observed for Pt/BEA S450 and Pt/BEA S550 results from the increased mobility of the sulfided Pt particles [32,33]. The lower intensity of the Pt–S contribution in the EXAFS of Pt/BEA S550 can be attributed to the generally lower concentration of sulfur retained and the reduced fraction of exposed metals.

4.2. Impact of the sulfur treatment on the acidic properties

The acid–base properties of the parent Pt/BEA varied drastically with the H_2S and oxidation treatment applied. NH_3 TPD revealed that the concentration and strength of acid sites first increased compared with the parent Pt/BEA (Pt/BEA S350, Pt/BEA S450) and then decreased (Pt/BEA S550) (see Fig. 3). However, the decrease in the strongly held NH_3 (desorbing at higher temperatures during TPD) and the increase in the more weakly held NH_3 (desorbing at lower temperatures during TPD) suggests that sulfation reduced the concentration of the strongest acid sites and increased the sites of weak and moderate acid strength.

In situ IR spectroscopy showed a new band at 1385 cm^{-1} assigned to the asymmetric stretching frequency of S=O in surface sulfate [23,24], which was more intense at lower sulfation temperatures. The downward shift of the bands of the S=O

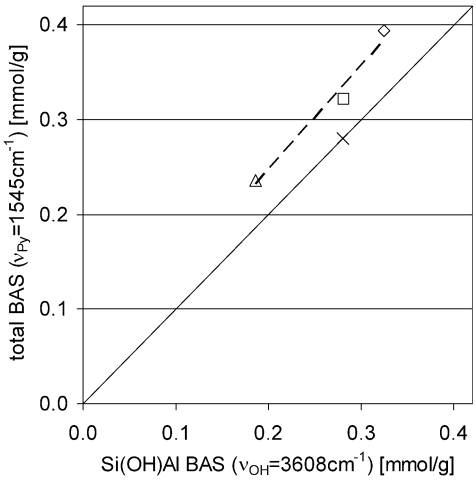

Fig. 15. Correlation between the concentration of Brønsted acid sites determined by adsorption of pyridine with the concentration of Si(OH)Al groups; the symbols denote Pt/BEA (×), Pt/BEA S350 (◇), Pt/BEA S450 (□) and Pt/BEA S550 (△).

stretching vibration of these sulfate groups after adsorption of pyridine suggests that the sulfates interact directly or indirectly with pyridine and that all are accessible to this base (see Figs. 5 and 6).

The ring vibrations of adsorbed pyridine indicate the presence of strong Brønsted acid sites as well as Lewis acids associated with accessible Al^{3+} cations in all materials studied. The higher concentration of Brønsted acid sites in Pt/BEA S350 and Pt/BEA S450 compared with the parent sample detected in this way suggests a direct and marked impact of the sulfation treatment, while the concentration of Lewis acid-bound pyridine hardly varied.

In principal, the increased concentration of Brønsted acid sites could be caused by one of two effects: (i) the formation of new Brønsted acidic OH groups affiliated with sulfate groups or (ii) the removal of cationic alumina species from ion-exchange sites (forming sulfates), making zeolite SiOHAl groups accessible. Because the OH groups of zeolite BEA are well-defined, the comparison between the intensities of the SiOHAl groups and the concentration of the pyridinium ions can be used to differentiate between these two options (see Fig. 15). In this figure, the total concentration of the Brønsted acid sites, calculated from the molar extinction coefficient for the band at 1544 cm^{-1} published by Emeis [20] is directly correlated with the intensity of the OH band at 3608 cm^{-1} (bridging hydroxy groups), allowing determination of an apparent molar extinction coefficient for the SiOHAl band at 3608 cm^{-1} normalized to the lattice vibration. For the sulfated samples, this extinction coefficient was used to determine the expected concentration of Brønsted acid sites from the concentration of SiOHAl groups present. For all three sulfate-treated samples, a clear correlation can be seen between the intensity of the band for the OH groups and the band of the pyridinium ions. The parent sample and Pt/BEA S450 exhibited the same intensity of the bridging OH band, but Pt/BEA S450 had a higher concentration of pyridinium ions. This suggests that, at least in this sample, Brønsted acid sites that are not part of the zeolite OH groups must exist after sulfation. On the other hand, in Pt/BEA S350 the concentration of zeolite OH groups was increased (as judged by the OH band at 3608 cm^{-1}) compared with the parent sample, indicating that the treatment removed some of the anionic aluminum oxide clusters that compensate for the charge of Al–O tetrahedra in the parent material. Thus, we conclude that the sulfate treatment has two effects under optimal preparation conditions: (i) creating new acidic OH groups in the zeolite by removing oxide clusters blocking acid sites and (ii) creating new OH groups affiliated with sulfate that are not readily detected because of hydrogen bonding [34]. Extrapolating, the trend line observed with the sulfur-treated samples appears to be parallel to the trend line known for the correlation of bridging hydroxy groups in zeolites and the concentration of adsorbed base molecules. This suggests that a constant concentration of Brønsted acidic SO_4 groups is formed in this material, which generates approximately 0.05 mmol/g Brønsted acid sites independent of the treatment.

At higher sulfation temperatures (Pt/BEA S550), the additional silanol groups at 3733 cm^{-1}, assigned to SiOH groups at defects, and the severely reduced band at 3608 cm^{-1} indicate the partial destruction of the zeolite framework. At this point, it is interesting to note that sulfuric acid is thermodynamically stable only up to 350 °C. Thus, the enhancement of bridging hydroxyl groups by the leaching of extra-framework alumina species from the ion-exchanged sites with in situ-formed (mobile) surface sulfates is more likely at a sulfation temperature of 350 °C.

The fact that sulfate species have strong Brønsted acidity and thus enhance the concentration of acid sites can be explained by the conversion of $(AlO)_3S{=}O$ groups to Brønsted acidic $(AlO)_2SOO^-H^+$ groups in the presence of water or OH groups [23]. The S–OH groups are usually strongly hydrogen-bonded to the surface lead generating very broad OH bands [34].

4.3. Catalytic properties

Pentane hydroisomerization proceeds on bifunctional Pt-containing zeolites via dehydrogenation on the metal, followed by isomerization via carbenium ions on Brønsted acid sites and a final hydrogenation on the metal [35,36]. Therefore, the activity and selectivity of the bifunctional catalyst depend on the ratio of metal to acid sites, which determines the concentration of olefins and carbenium ions on the catalyst surface.

The linear region in the Arrhenius plots at temperatures below 300 °C (shown in Fig. 9) suggests the absence of pore diffusion limitations in the BEA-based catalysts studied here under the reaction conditions used here. Compared with the parent sample, hydroisomerization activity was higher for Pt/BEA S350 and Pt/BEA S450 and lower for Pt/BEA S550. Linear correlation of the Brønsted acid site concentration and the catalytic activity of Pt/BEA, Pt/BEA S350, and Pt/BEA S450 suggests that the rate-determining step of the reaction over these materials is rearrangement of the carbenium ion on the acid site (Fig. 10). The deviation observed for Pt/BEA S550 indicates a shift in the rate-determining step toward dehydrogenation on the metal resulting from a reduction in the metal atoms exposed.

Therefore, the activity of this catalyst was only about half of what would be expected for a catalyst with corresponding acidity. The small changes in the apparent activation energies for the catalyst before and after sulfur treatment are in agreement with the subtle variations in acid strengths observed on ammonia TPD.

Besides the enhanced activity of the catalysts after sulfur treatment, a significant improvement in the selectivity to isopentane (i.e., a reduction of the formation of light alkanes) was observed. The reaction to these latter products can be caused by metal-catalyzed hydrogenolysis or hydrocracking also involving acid catalysis. The product distribution as a function of Pt/BEA conversion was symmetric with respect to the concentrations of C_2 and C_3 as well as C_1 and C_4 fragments. The products were similar to those observed with Pt/ASA. This support is only weakly acidic (0.065 mmol H^+/g) and showed no significant activity for the pentane isomerization reaction (Fig. 12).

Two possible reaction routes can lead to light alkanes: bifunctional hydrocracking and metal-catalyzed hydrogenolysis. In bifunctional hydrocracking, the side reaction occurs on the acid sites, and the metal compound acts to dehydrogenate pentane and hydrogenate the olefins formed from the acid-catalyzed cracking of the olefins. The selectivity enhancement after sulfation could be explained by the reduced strength of the Brønsted acid sites, as evidenced by TPD of ammonia. The weaker Brønsted acid sites retain less alkenes, leading to a lower fraction of cracked molecules. Whereas the shift from cracking to isomerization is well established, changes in the distribution of acid sites are rather subtle, and it is difficult to accept (but cannot be ruled out) that such a subtle change (with only a fraction of the sites of reduced strength) can lead to such a pronounced modification of catalytic properties.

Hydrogenolysis, the second possible pathway to light alkanes, occurs only on the metal. A reduction in available metal surface atoms would lead to a severely reduced rate of this structure-sensitive reaction. It has been argued that hydrogenolysis requires larger ensembles of metal atoms or the presence of highly uncoordinated metal atoms, because the reaction involves dehydrogenated intermediates with multiple bonds to the metal particle [37]. Both free ensembles of Pt atoms and highly reactive and exposed metal atoms would be dramatically reduced by the presence of sulfur on the metal.

In contrast, hydrogenation/dehydrogenation is less demanding with respect to the number, arrangement, and reactivity of metal surface atoms, and so it is conceivable that sulfur treatment blocks the sites required for hydrogenolysis while leaving a sufficiently high concentration of Pt sites to maintain the hydrogenation/dehydrogenation equilibrium on the bifunctional catalysts. Note that in Pt/BEA S550, this concentration is so low that hydrogenation/dehydrogenation cannot be in equilibrium.

5. Conclusions

Sequential treatment with H_2S and air severely modifies the acidic and metallic properties of the bifunctional catalyst based on Pt-containing zeolite BEA. We have shown that it is possible to enhance the concentration of Brønsted acid sites of the sample at low sulfation temperatures. The enhancement of Brønsted acid sites can be attributed to the removal of cationic alumina species blocking ion-exchange sites and to the formation of additional Brønsted acidic sulfate species. When the procedure was carried out at 550 °C, the concentration of Brønsted acid sites was reduced by dealumination.

The presence of sulfur species reduces the available metal surface atoms compared with the parent material. Although sulfur exists on the surface in all samples, the oxidation state of this sulfur seems to depend strongly on the atmosphere; that is, in a reducing atmosphere, sulfide species are likely formed. For Pt/BEA S350 and Pt/BEA S450, the reduction of available Pt surface atoms from decoration of the Pt particles with sulfur atoms is the dominating effect. In contrast, for Pt/BEA S550, sulfation decreased the available metal surface area due to chemisorbed sulfur species and sintering of the Pt particles.

Isomerization activity was significantly enhanced for materials treated with H_2S/air up to 450 °C. For the parent material and these new catalysts, isomerization activity was directly correlated with the concentration of Brønsted acid sites, indicating that the carbenium ion chemistry is rate-determining. For Pt/BEA S550, the concentration of metal sites remaining was insufficient to equilibrate the hydrogenation/dehydrogenation step, causing an overall rate decrease. The selectivity of the sulfur-treated catalyst was dramatically increased to near-100% isomerization. Although we cannot completely exclude the role of the modified Brønsted acid sites in this mechanism, we do believe that the modification of the metal particles by sulfur species eliminates the hydrogenolysis of alkanes observed with the parent sample.

Therefore, the approach described herein offers a promising new route for tailoring zeolite-based bifunctional catalysts. The experimental conditions should be as mild as possible, to maintain the structural integrity of both catalyst components.

Acknowledgments

Financial support was provided by Bundesministerium für Bildung und Forschung Project (BMBF:03C0307D). The XAFS experiments were carried out at HASYLAB, DESY, Hamburg, Germany and supported by TMR contract ERBFMGECT950059 of the European Community. The authors thank Xaver Hecht for H_2-chemisorption measurements and technical support on the 20-fold parallel reactor system, and Hendrik Dathe for stimulating discussions on XAS and the nature of sulfate species.

References

[1] M. Guisnet, N.S. Gnep, Appl. Catal. A: Gen. 146 (1996) 33.
[2] A. Corma, J. Planelles, J. Sanchez-Marin, F. Thomas, J. Catal. 93 (1985) 30.
[3] H.-C. Wu, L.-J. Leu, C. Naccache, K.-J. Chao, J. Mol. Catal. A: Chem. 127 (1997) 1143.
[4] N. Essayem, Y.B. Taârit, C. Feche, P.Y. Gayraud, G. Sapaly, C. Naccache, J. Catal. 219 (2003) 97.

[5] S. Kuba, P. Lukinskas, R.K. Grasselli, B.C. Gates, H. Knözinger, J. Catal. 216 (2002) 353.
[6] Y. Ono, Catal. Today 81 (2003) 3.
[7] US Patent no. 5,157,199 (1992).
[8] US Patent no. 6,107,235 (2000).
[9] K.-J. Chao, H.-C. Wu, L.-J. Leu, Appl. Catal. A: Gen. 143 (1996) 223.
[10] M.A. Saberi, R.L. Van Mao, M. Martin, A.W.H. Mak, Appl. Catal. A: Gen. 214 (2001) 229.
[11] M.A. Saberi, R.L. Van Mao, Appl. Catal. A: Gen. 242 (2003) 139.
[12] T. Lei, J.S. Xu, Z. Gao, Mater. Chem. Phys. 60 (1999) 177.
[13] C.P. Hubbard, K. Otto, H.S. Gandhi, K.Y.S. Ng, J. Catal. 144 (1993) 484.
[14] A.F. Lee, K. Wilson, R.M. Lambert, C.P. Hubbard, R.G. Hurley, R.W. McCabe, H.S. Gandhi, J. Catal. 184 (1999) 491.
[15] R. Burch, E. Haplin, M. Hayes, K. Ruth, J.A. Sullivan, Appl. Catal. B: Environ. 19 (1998) 199.
[16] J.M. Jones, V.A. Dupont, R. Brydson, D.J. Fullerton, N.S. Nasri, A.B. Ross, A.V.K. Westwood, Catal. Today 81 (2003) 589.
[17] A.L. Ankudinov, J.J. Rehr, Phys. Rev. B 62 (2000) 2437.
[18] K.V. Klementiev, VIPER for Windows, freeware, http://www.desy.de/~klmn/viper.html;
K.V. Klementiev, J. Phys. D: Appl. Phys. 34 (2001) 209.
[19] J.A. Lercher, Ch. Gründling, G. Eder-Mirth, Catal. Today 27 (1996) 353.
[20] C.A. Emeis, J. Catal. 141 (1993) 347.
[21] C.L. Garcia, J.A. Lercher, J. Phys. Chem. 96 (1992) 2230.
[22] A. Jentys, Phys. Chem. Chem. Phys. 1 (1999) 4059.
[23] O. Saur, M. Bensitel, A.B.M. Saad, J.C. Lavalley, C.P. Tripp, B.A. Morrow, J. Catal. 99 (1986) 104.
[24] T. Yamaguchi, T. Jin, K. Tanabe, J. Phys. Chem. 90 (1986) 3148.
[25] X. Li, K. Nagaoka, J.A. Lercher, J. Catal. 227 (2004) 130.
[26] M.A. Babaeva, A.A. Tsyganenko, Kinet. Catal. 25 (1985) 787.
[27] M.B. Mitchell, V.N. Sheinker, J. Phys. Chem. 100 (1996) 7550.
[28] J.A. Wang, L.F. Chen, R. Limas-Ballesteros, A. Montoya, J.M. Dominguez, J. Mol. Catal. A: Chem. 194 (2003) 181.
[29] J. de Graaf, A.J. van Dillen, K.P. de Jong, D.C. Koningsberger, J. Catal. 203 (2001) 307.
[30] S. Feast, M. Englisch, A. Jentys, J.A. Lercher, Appl. Catal. A: Gen. 174 (1998) 155.
[31] M. Vaarkamp, J.T. Miller, F.S. Modica, G.S. Lane, D.C. Koningsberger, J. Catal. 138 (1992) 675.
[32] J.-R. Chang, S.-L. Chang, T.-B. Lin, J. Catal. 169 (1997) 338.
[33] J.-R. Chang, S.-L. Chang, J. Catal. 176 (1998) 42.
[34] X. Li, K. Nagaoka, J.A. Lercher, J. Catal. 227 (2004) 130.
[35] P.B. Weisz, Adv. Catal. 13 (1962) 137.
[36] F.J.M. M de Gauw, J. Grondelle, R.A. van Santen, J. Catal. 206 (2002) 295.
[37] E.H. Van Broekhoven, V. Ponec, J. Mol. Catal. 25 (1984) 109.